Catal Lett (2012) 142:32–41
DOI 10.1007/s10562-011-0724-x

Synthesis of Highly Effective CeO_x–MnO_y–BaO Catalysts for Direct NO Decomposition

Won-Jong Hong · Mao Ueda · Shinji Iwamoto · Saburo Hosokawa · Kenji Wada · Masashi Inoue

Received: 17 May 2011 / Accepted: 18 October 2011 / Published online: 3 November 2011

Abstract Ce–Mn mixed oxides with a Mn/(Ce + Mn) molar ratio of 0.25 were prepared by solvothermal (ST-1) and co-precipitation (CP) methods, and Ba was loaded on the Ce–Mn oxides. In addition, CeO_2–MnO_x–BaO catalysts with various compositions were directly prepared by the solvothermal (ST-2) method. The NO decomposition activities of these catalysts were examined. Among the catalysts examined, the ST-2 catalyst having a nominal composition of $Ce_{0.8}Mn_{0.15}Ba_{0.05}O_x$ exhibited the highest activity; 77% NO conversion to N_2 was attained at 800 °C. These catalysts were characterized by X-ray diffraction, Raman spectroscopy, and X-ray photoelectron spectroscopy (XPS). The Raman and XPS results indicate that the CP catalyst had larger amounts of the $BaMnO_{3-\delta}$ and/or Mn_3O_4 phases. The ST-1 and ST-2 catalysts had highly dispersed Ba species on the surface. The ST-2 catalyst had Mn species with the lowest binding energy of Mn 2p and also had a high population of oxygen vacancies in the ceria lattice, suggesting that Mn species with a low oxidation state contributes to the formation of oxygen vacancies, which play an important role in this reaction.

W.-J. Hong · M. Ueda · S. Hosokawa · K. Wada · M. Inoue (✉)
Department of Energy and Hydrocarbon Chemistry, Graduate School of Engineering, Kyoto University, Katsura, Kyoto 615-8510, Japan
e-mail: inoue@scl.kyoto-u.ac.jp

S. Iwamoto
Department of Chemistry and Chemical Biology, Graduate School of Engineering, Gunma University, Tenjin, Kiryu 376-8515, Japan

Keywords Ceria · Manganese oxide · Barium · Mixed oxide catalysts · Direct NO decomposition · Solvothermal method

1 Introduction

Cerium oxide and CeO_2-containing materials are well known as catalysts for various reactions or as structural and electronical promoters for catalysts [1]. Cerium oxide has the ability to store and release oxygen by the redox cycle of cerium ions. When cerium oxide is combined with transition metal oxides, the composite oxide catalysts have improved redox properties by the formation of surface and bulk oxygen vacancies. Among the numerous ceria-based catalysts, MnO_x–CeO_2 catalysts have been found to be remarkably active for wet oxidation of phenol [2], SCR of NO with NH_3 [3], and catalytic NO_x sorption [4] as well as oxidation of ethanol [5], formaldehyde [6], toluene [7], *o*-xylene [8], and VOC [9]. The MnO_x–CeO_2 solid solutions have been prepared by various methods, i.e., co-precipitation [2–4, 6, 8, 10], citric acid sol–gel [5–7, 10], wet-impregnation [10], and solution combustion [9, 11] methods. For example, Chen et al. [2] prepared Mn–Ce–O composites with various atomic ratios by co-precipitation methods and showed on the basis of X-ray diffraction (XRD) and X-ray photoelectron spectroscopy (XPS) results that Mn ions are incorporated in the fluorite structure of ceria. Qi and Yang [10] examined the preparation of MnO_x–CeO_2 by citric acid sol–gel, impregnation, and co-precipitation methods and reported that three types of Mn phases were present in a MnO_x–CeO_2 sample with the composition ratio of Mn/(Ce + Mn) = 0.3 prepared by the citric acid sol–gel method; (1) aggregated MnO_x species on the surface of CeO_2, (2) highly dispersed MnO_x with strong interaction

with CeO_2, and (3) Mn atoms incorporated into the CeO_2 lattice. Kaneko et al. [11] examined the formation of $Ce_{0.9}Mn_{0.1}O_{2-\delta}$ solid solutions by a solution combustion method and observed an expansion of the lattice compared to pure ceria. They suggested that the $Ce_{0.9}Mn_{0.1}O_{2-\delta}$ solid solution had an oxygen-deficient structure, cation repulsion causing the expansion of the fluorite lattice.

Nitrogen oxides (NO_x) formed by combustion cause severe environmental problems such as acid rain and photochemical smog. Catalytic NO_x reduction processes such as three-way catalysts for gasoline-fueled vehicles, NO_x storage–reduction (NSR) catalysts for lean-burn engines, and selective catalytic reduction with ammonia (SCR) for large-scale combustion facilities have been developed. The concentration of NO_x in the atmosphere in urban areas, however, has significantly increased recently; therefore, the development of other effective deNO_x methods is desired. Among various deNO_x strategies, direct decomposition of NO ($2NO \rightarrow O_2 + N_2$) is expected to be the most desirable because this process is quite simple and does not need any reductants such as NH_3, H_2, CO, or hydrocarbons.

Catalysts, such as precious metals [12–14], single metal oxides [15, 16], Cu-ZSM-5 [17–19], alkali-doped Co_3O_4 [20, 21], perovskites [22–26], C-type cubic rare earth oxides [27, 28], and $Ba_{0.5}/BaY_2O_4$ [29], have been found to be effective for direct decomposition of NO. We found that Ba–Ce–Co mixed oxides prepared by a polymerized complex method showed high NO decomposition activities [30]. The addition of other components to CeO_2 was also examined, and it was found that Ce–Mn mixed oxides modified with Ba species showed improved activities [31].

In this study, the Ce–Mn mixed oxides and the CeO_x–MnO_y–BaO catalysts were prepared by various methods, and the effect of the preparation methods on the physical properties of these materials were examined aiming to find a suitable method for the preparation of the catalyst having high performance for direct decomposition of NO.

2 Experimental

2.1 Preparation of the Catalysts

The Ce–Mn mixed oxide samples were prepared by three different methods (Scheme 1). (1) *Co-precipitation method (denoted as CP)*. $Ce(NO_3)_3{\cdot}6H_2O$ (16.28 g) and $Mn(NO_3)_2{\cdot}6H_2O$ (3.58 g; Mn/(Ce + Mn) molar ratio, 0.25) were dissolved in 100 mL of deionized water. To this solution, the aqueous solution (200 mL) of a base (NH_3, $NaHCO_3$, NH_4HCO_3, or $(NH_4)_2CO_3$) was added at once at room temperature with vigorous stirring, and the mixture was stirred for 1 h. The precipitate was centrifuged and washed with deionized water, followed by drying at 80 °C. The precursor was calcined at 400 °C for 4 h.

(2) *Solvothermal method-1 (denoted as ST-1)*. $Ce(CH_3COO)_3{\cdot}H_2O$ (12.6 g) and $Mn(CH_3COO)_2{\cdot}4H_2O$ (3.07 g; Mn/(Ce + Mn) = 0.25) were added to 100 mL of an organic solvent (2-methylaminoethanol, 2-dimethylaminoethanol, 1-dodecanol, 1-hexanol, 1,6-hexanediol, 1,4-butanediol, 1,2-butanediol, or ethylene glycol), and this mixture was placed in a 300-mL autoclave. After the autoclave was purged with nitrogen, the mixture was heated to 300 °C at a rate of 2.3 °C min^{-1} and kept at that temperature for 2 h. After the autoclave was cooled to room temperature, the resultant powder product was collected by centrifugation. It was washed with acetone, air-dried, and then calcined in air at 400 °C for 4 h.

Barium was loaded on the Ce–Mn mixed oxides (prepared by ST-1 or CP) by an impregnation method using an aqueous solution of barium nitrate, followed by calcination at 800 °C for 1 h. The barium loading (as BaO) was adjusted to 7 wt% [32]. These catalysts were denoted as CP(formula of the precipitant) or ST-1(name of the solvent).

(3) *Solvothermal method-2 (denoted as ST-2)*. Catalysts having various compositions were prepared by solvothermal treatment of all the starting materials in 1,4-butanediol followed by calcination. Appropriate amounts of $Ce(CH_3COO)_3{\cdot}H_2O$, $Mn(CH_3COO)_2{\cdot}4H_2O$ and $Ba(CH_3COO)_2$ were added to 100 mL of 1,4-butanediol, and this mixture was set in a 300-mL autoclave. After the autoclave was purged with nitrogen, the mixture was heated to 300 °C at a rate of 2.3 °C min^{-1} and kept at that temperature for 2 h. After the autoclave was cooled to room temperature, the resultant powder product was collected by centrifugation. It was washed with acetone, air-dried, and then calcined in air at 800 °C for 1 h. These catalysts were denoted as ST-2($Ce_{1-a-b}Mn_aBa_bO_x$) where *a* and *b* stand for the starting compositions of Mn and Ba.

2.2 Direct NO Decomposition

Catalytic tests for the NO decomposition reaction were carried out in a fixed-bed flow reactor of quartz glass tubing with an inner diameter of 10 mm. The catalyst (0.50 g), after being pressed into a pellet and pulverized into 10–22 mesh size, was placed in the reactor. The catalyst bed was heated to 550 °C in a helium flow and held at that temperature for 30 min. Then, the reaction gas composed of 6,000 ppm NO and helium balance was introduced to the catalyst bed at 30 mL min^{-1} ($W/F = 1.0$ g s mL^{-1}). The reaction temperature was increased from 550 to 800 °C at 5 °C min^{-1} and kept for 15 min at every 50 °C interval to attain the stationary state. The effluent gas was analyzed using a gas chromatograph (GL Sciences,

Scheme 1 Preparation of the catalysts

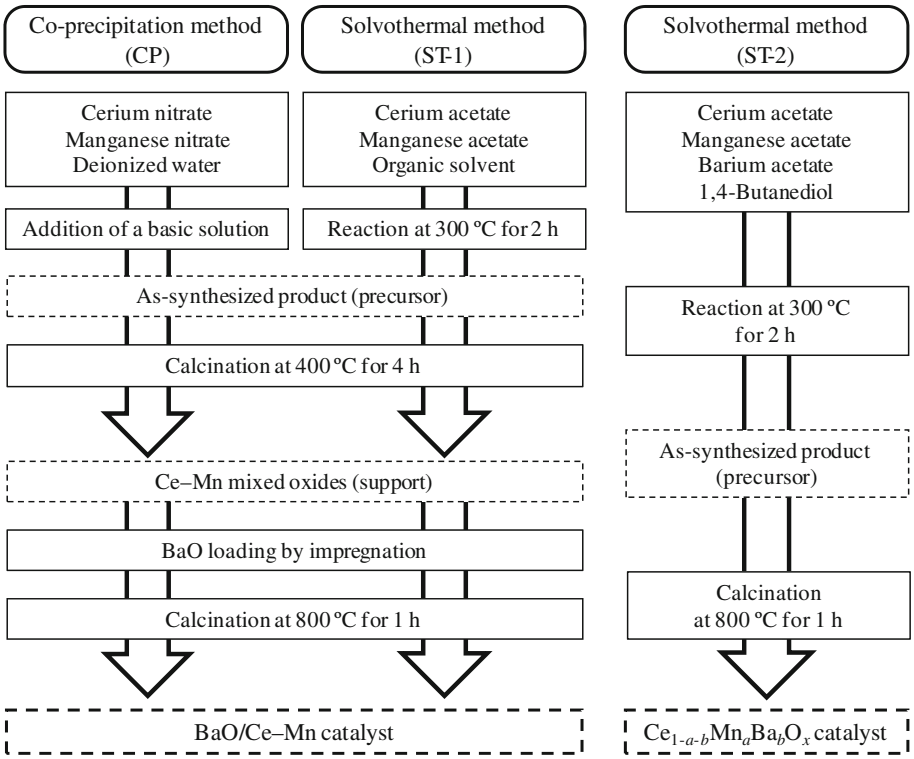

MicroGC 2002) equipped with Molsieve 5A and Poraplot Q columns. The NO conversion is expressed on the basis of the formation of N_2:

$$\text{NO conversion} = \frac{2[N_2]_{out}}{[NO]_{in}},$$

where $[N_2]_{out}$ and $[NO]_{in}$ are the N_2 concentration in the exhaust and the NO concentration in the feed, respectively.

In the present study, only small amounts of the by-product, N_2O (<50 ppm), were observed for all the catalysts tested.

2.3 Characterization of the Catalysts

Powder XRD patterns were recorded on a Shimadzu XD-D1 diffractometer using Cu Kα radiation and a carbon-monochromator.

Specific surface areas of the catalysts were calculated by the BET single-point method on the basis of nitrogen uptake measured at 77 K using a Micromeritics Flowsorb II 2300 sorptograph.

Raman spectra were recorded on a Jobin–Yvon T64000 Raman spectrometer at room temperature using a 514.5 nm argon laser.

The bulk compositions were analyzed with a Shimadzu ICPS-1000IV inductively coupled plasma atomic emission spectrometer (ICP-AES). The catalysts were dissolved in phosphoric acid at 80 °C followed by dilution to about 0.2 g L^{-1} with water. The surface compositions were determined with an ULVAC-PHI 5500 XPS instrument with a hemispherical energy analyzer. Samples were mounted on a piece of indium foil, and then transferred to the XPS analyzer chamber. The residual gas pressure in the chamber during data acquisition was less than 1×10^{-8} Torr (1 Torr = 133.3 N m^{-2}). The spectra were measured at room temperature using Mg Kα radiation (15 kV, 400 W). Binding energies (BE) were calibrated on the basis of the C 1 s BE (284.6 eV) of the residual carbon.

3 Results and Discussion

3.1 Phases Detected by XRD

The properties of the precursors for the Ce–Mn mixed oxide supports before calcination (denoted as precursors), Ce–Mn mixed oxides calcined at 400 °C (supports), and Ba-loaded Ce–Mn mixed oxides (catalysts) were evaluated by means of XRD. Figure 1 shows the XRD patterns of the precursors (Fig. 1A), supports (Fig. 1B), and catalysts (Fig. 1C) obtained by the CP method using various bases. Only CeO_2 with a cubic fluorite structure (JCPDS #34-0394) was detected in the precursors obtained by the use of NH_3 and $(NH_4)_2CO_3$, while the use of $NaHCO_3$ and NH_4HCO_3 produced $Ce_2(CO_3)_3{\cdot}6H_2O$ (JCPDS #30-0295) and $MnCO_3$ (JCPDS #07-0268) phases, respectively. Diffraction peaks due to the CeO_2 phase were recognized for all the supports (Fig. 1B) and catalysts (Fig. 1C). For the catalysts,

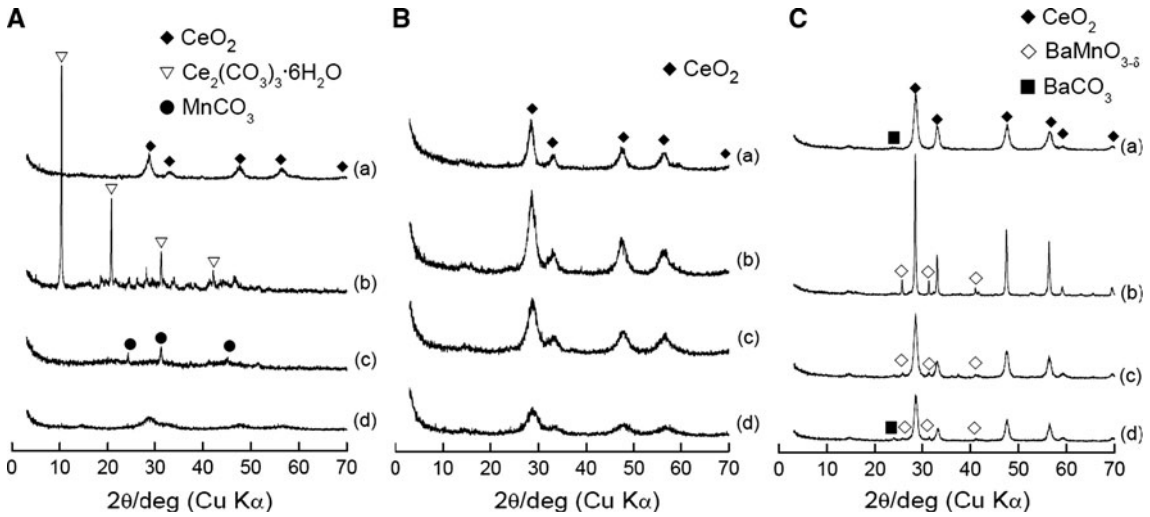

Fig. 1 XRD patterns of the precursors (**A**), supports (**B**), and catalysts (**C**) prepared by CP method using: (*a*), NH_3; (*b*), $NaHCO_3$; (*c*), NH_4HCO_3; (*d*), $(NH_4)_2CO_3$; as precipitants

diffraction peaks due to $BaMnO_{3-\delta}$ (JCPDS #26-0170) were also observed; especially, CP($NaHCO_3$) exhibited these peaks with stronger intensities as compared with the other CP catalysts. Diffraction peaks due to $BaCO_3$ (JCPDS #45-1471) were also detected in the CP(NH_3) and CP($(NH_4)_2CO_3$) catalysts. These results indicate that Ba ions in these CP catalysts were not dispersed well.

Figures 2 and 3 show the XRD patterns of the ST-1 and ST-2 samples. For the precursors of ST-1 (Fig. 2A) and ST-2 (Fig. 3A), diffraction peaks due to two modifications of cerium acetate oxide ($Ce(CH_3COO)O$, AOA and AOB) [33–35], cerium diacetate hydroxide ($Ce(CH_3COO)_2(OH)$, DAH) [33–35], $Ce(CO_3)OH$ (JCPDS #41-0013) and/or $Ce_2O(OCH_2CH_2O)(CH_3COO)_2$ [34] were observed (Table 1). The last phase was obtained by the reaction of cerium acetate alone in ethylene glycol. These results indicate that the solvent used in the solvothermal method affected the crystalline phase of the precursors. Diffraction peaks due to the CeO_2 phase were recognized for all the ST-1 supports as well as ST-1 and ST-2 catalysts. For some of the ST-1 and ST-2 catalysts, diffraction peaks due to the $BaMnO_{3-\delta}$ phase were observed in addition to the CeO_2 peaks. Moreover, diffraction peaks due to $BaCO_3$ were also detected in some of the ST-2 catalysts (Fig. 3B (e, f, and h)), indicating that Ba ions were not dispersed well in these catalysts.

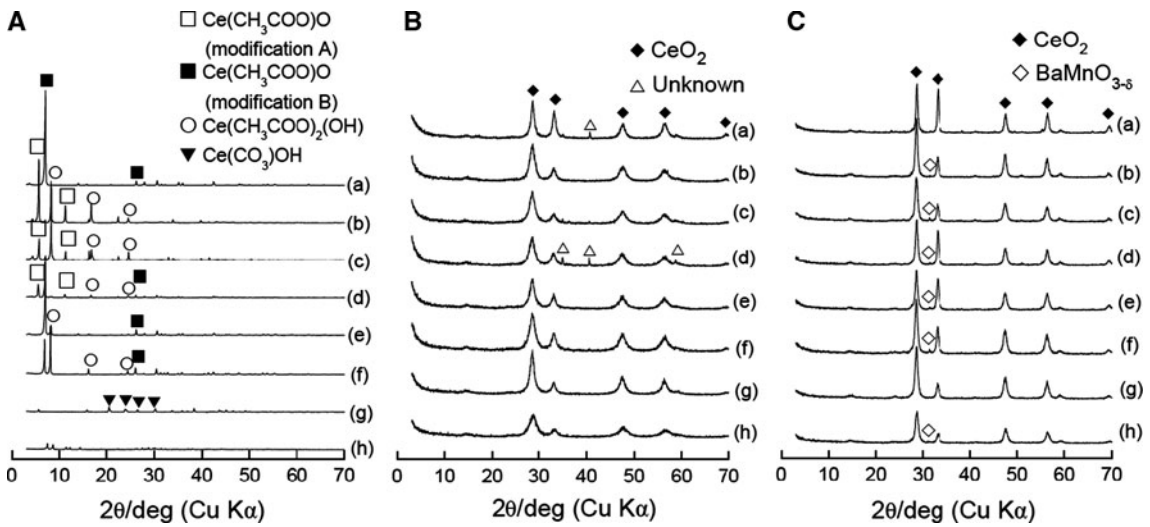

Fig. 2 XRD patterns of the precursors (**A**), supports (**B**), and catalysts (**C**) prepared by ST-1 method using: (*a*), 2-methylaminoethanol; (*b*), 2-dimethylaminoethanol; (*c*), 1-dodecanol; (*d*), 1-hexanol; (*e*), 1,6-hexanediol; (*f*), 1,4-butanediol; (*g*), 1,2-butanediol; (*h*), ethylene glycol; as solvents

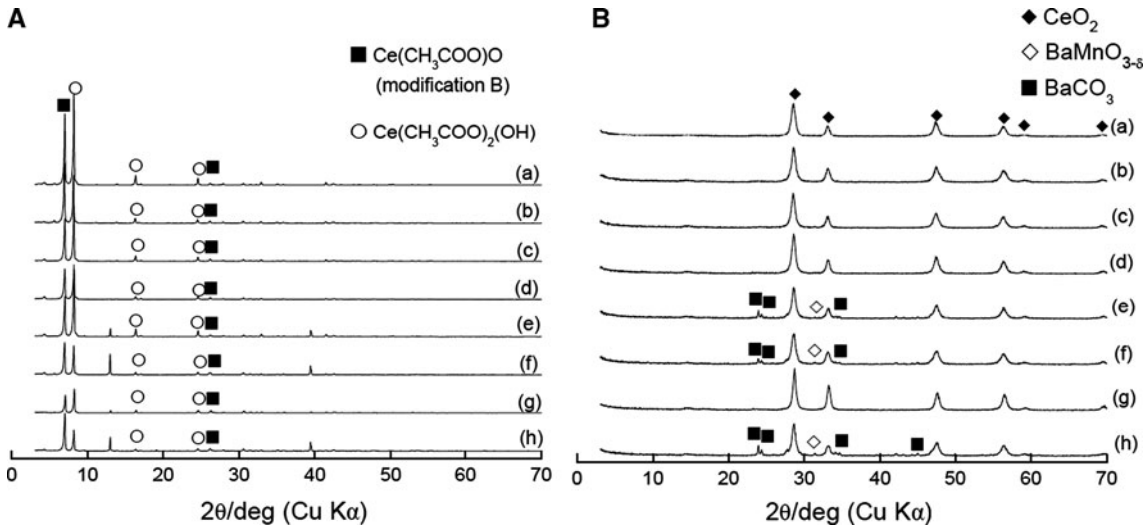

Fig. 3 XRD patterns of the precursors (**A**), and catalysts (**B**) prepared by ST-2 method having the nominal compositions of: (*a*), $Ce_{0.83}Mn_{0.15}Ba_{0.02}O_x$; (*b*), $Ce_{0.8}Mn_{0.18}Ba_{0.02}O_x$,; (*c*), $Ce_{0.8}Mn_{0.15}Ba_{0.05}O_x$; (*d*), $Ce_{0.75}Mn_{0.23}Ba_{0.02}O_x$; (*e*), $Ce_{0.7}Mn_{0.1}Ba_{0.2}O_x$; (*f*), $Ce_{0.7}Mn_{0.2}Ba_{0.1}O_x$; (*g*), $Ce_{0.7}Mn_{0.23}Ba_{0.07}O_x$; (*h*), $Ce_{0.6}Mn_{0.2}Ba_{0.2}O_x$

Table 1 Phases in the precursors obtained by the solvothermal reactions in various solvents

Sample		Precursor phase[a]
ST-1	2-methylaminoethanol	AOB
	2-dimethylaminoethanol	AOA, DAH
	1-dodecanol	AOA, DAH
	1-hexanol	AOB, AOB, DAH
	1,6-hexanediol	AOB, DAH
	1,4-butanediol	AOB, DAH
	1,2-butanediol	$CeCO_3OH$
	Ethylene glycol	$Ce_2O(OCH_2CH_2O)(CH_3COO)_2$
ST-2	$Ce_{1-a-b}Mn_aBa_bO_x$	AOB, DAH

[a] DAH, ceriume diacetate hydroxide, Ce(CH3COO)2(OH); AOA and AOB, cerium acetate oxide (Ce(CH3COO)O) with two different structures

3.2 NO Decomposition Activities of the Catalysts Prepared by Various Methods

Table 2 summarizes the NO decomposition activities of the CP, ST-1, and ST-2 catalysts. Among the CP catalysts examined, CP($(NH_4)_2CO_3$) exhibited the highest activity, and 53% NO conversion was attained at 800 °C. However, the activities of the CP catalysts were lower than those of the ST-1 and ST-2 catalysts, and had no correlation with BET surface areas. On the other hand, the NO decomposition activities of the ST-1 catalysts are well correlated with their BET surface areas (Table 2): The ST-1 catalysts prepared by using 1,4-butanediol and 1,6-hexanediol had large BET surfaces areas and exhibited excellent activities.

Among the ST-2 catalysts having various compositions, the highest activity (77% of NO conversion to N_2 at 800 °C) was attained by the ST-2($Ce_{0.8}Mn_{0.15}Ba_{0.05}O_x$) catalyst, while Ba-poor catalysts exhibited relatively low activities (Table 2).

Figure 4 shows the comparison of the activities of the catalysts that exhibited the highest activities among the catalysts prepared by each method. Although the activity of the ST-1(1,6-hexanediol) was comparable to that of ST-1(1,4-butanediol), the latter catalyst was predominantly used for the work hereafter because of difficulty in the synthesis of the former catalyst: Since 1,6-hexanediol has a high melting point (42.9 °C), extensive washing is required to remove the solvent from the solvothermal product.

The ST-2($Ce_{0.8}Mn_{0.15}Ba_{0.05}O_x$) (▲) catalyst showed higher NO conversion than the ST-1(1,4-butanediol) (□) and CP($(NH_4)_2CO_3$) (●) catalysts in the entire temperature range examined, and the ST-2 catalyst exhibited 13% of NO conversion to N_2 at 550 °C even though the reaction was carried out at a low *W/F* value (1.0 g s mL^{-1}). It should be noted that this temperature and the *W/F* value are much lower than those reported for other catalysts to obtain the same NO conversion [24–28]: For example, $La_{0.7}Ba_{0.3}Mn_{0.8}In_{0.2}O_3$ [24], $Ba_{0.8}La_{0.2}Mn_{0.8}Mg_{0.2}O_3$ [25], $LaSrMn_{1-x}Ni_xO_{4+\delta}$ [26], $(Gd_{0.70}Y_{0.26}Ba_{0.04})_2O_{2.96}$ [27], and $(Y_{0.69}Tb_{0.3}Ba_{0.01})_2O_{2.99+\delta}$ [28] catalysts were reported to exhibit ~12%, ~13%, <15%, ~10%, and ~5% NO conversion to N_2, respectively, at 600 °C under *W/F* of 3.0 g s mL^{-1}. On the other hand, ST-2($Ce_{0.8}Mn_{0.15}Ba_{0.05}O_x$) exhibited 45% NO conversion to N_2 under the same reaction conditions (Fig. 4(Δ)). This result implies that the present $Ce_{0.8}Mn_{0.15}Ba_{0.05}O_x$ catalyst may find some application in the future.

Table 2 BET surface areas and NO decomposition activities of the ST-1, ST-2, and CP catalysts

Sample		BET surface area ($m^2\ g^{-1}$)		NO conversion to N_2 (%)[a]	
		Supports[b]	Catalysts[c]	600 °C	800 °C
CP	NH_3	95	20	3	2
	$NaHCO_3$	13	2	4	12
	NH_4HCO_3	103	22	8	37
	$(NH_4)_2CO_3$	73	26	11	53
ST-1	2-methylaminoethanol	59	8	12	55
	2-dimethylaminoethanol	107	11	11	53
	1-dodecanol	99	14	14	55
	1-hexanol	107	13	17	64
	1,6-hexanediol	113	20	23	69
	1,4-butanediol	120	22	25	67
	1,2-butanediol	63	10	12	49
	Ethylene glycol	103	16	14	51
ST-2	$Ce_{0.83}Mn_{0.15}Ba_{0.02}O_x$	–	24	14	44
	$Ce_{0.8}Mn_{0.18}Ba_{0.02}O_x$	–	31	21	53
	$Ce_{0.8}Mn_{0.15}Ba_{0.05}O_x$	–	23	27	77
	$Ce_{0.75}Mn_{0.23}Ba_{0.02}O_x$	–	21	12	35
	$Ce_{0.7}Mn_{0.1}Ba_{0.2}O_x$	–	15	14	52
	$Ce_{0.7}Mn_{0.2}Ba_{0.1}O_x$	–	22	21	65
	$Ce_{0.7}Mn_{0.23}Ba_{0.07}O_x$	–	17	17	57
	$Ce_{0.6}Mn_{0.2}Ba_{0.2}O_x$	–	17	14	51

[a] Catalyst, 0.50 g; 6,000 ppm NO in He; $W/F = 1.0$ g s mL^{-1}

[b] Calcined at 400 °C

[c] Calcined at 800 °C

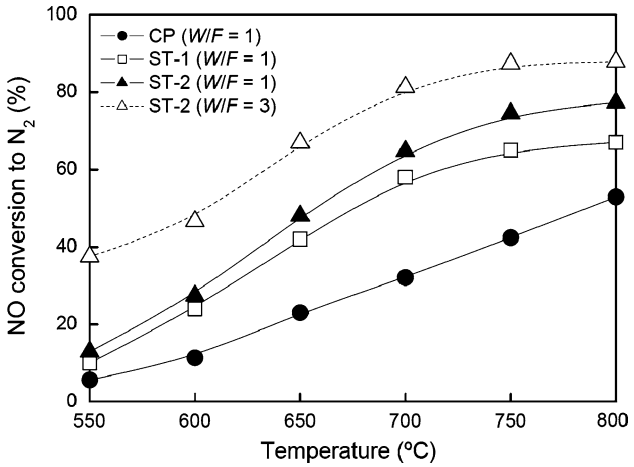

Fig. 4 Comparison of the activities of CP($(NH_4)_2CO_3$) (*filled circle*), ST-1(1,4-butanediol) (*open square*), and ST-2($Ce_{0.8}Mn_{0.15}Ba_{0.05}O_x$) (*filled triangle* and *open triangle*) catalysts for direct decomposition of NO under the conditions of 0.50 g catalyst and 6,000 ppm NO in He with the *W/F* value of: *filled circle*, *open triangle*, and *filled triangle*, 1.0; *open triangle*, 3.0 g s mL^{-1}

3.3 Characterization of the Catalysts Prepared by Various Methods

The bulk and surface compositions of the catalysts were investigated by the ICP-AES and XPS analyses, and the results are summarized in Table 3. The ICP-AES analysis showed that the catalysts had almost the same Mn contents as those of the starting materials, whereas the XPS results showed that the Mn concentrations in the surface region of the CP catalysts were larger than those expected from the starting compositions. The surface atomic ratio of the Ba species was found to be influenced by the preparation methods. Although the CP($(NH_4)_2CO_3$) catalyst had a relatively high surface Ba concentration (12%), the surface Ba concentrations of the other CP catalysts were low, and the activities of these catalysts seem to be determined by the surface Ba concentration. On the other hand, the surface Ba concentrations in ST-1(1,2-butanediol), ST-1(1-dodecanol), and ST-1(1,4-butanediol) catalysts were 16, 12, and 14%, respectively, while the nominal Ba content of the catalysts was 6%.

The ST-2($Ce_{0.8}Mn_{0.15}Ba_{0.05}O_x$) catalyst also had a high surface Ba concentration as compared with the nominal composition. Although the ST-2 catalysts were prepared by the reaction of Ce, Mn, and Ba starting reagents all together, the precursors for the ST-2 catalysts before calcination are composed of crystalline cerium acetate oxide and cerium diacetate hydroxide phases (Fig. 3), and Ba species seems not to be dissolved in these phases. Therefore, Ba species forms an amorphous phase which is highly dispersed on the outer surface of the intermediate phase. Calcination of this mixture gives Ce–Mn mixed oxide and a part of the Ba ions migrates in the lattice of the mixed oxide [36]. This situation is almost the same as the ST-1 synthesis, and therefore, surface Ba contents of the ST-1

Table 3 Composition of the ST-1, ST-2, and CP catalysts

Sample		Nominal (%) Ce/Mn/Ba	ICP analysis (%) Ce/Mn/Ba	XPS analysis (%) Ce/Mn/Ba
CP	NH_3	71/23/6	77/20/3	67/31/2
	$NaHCO_3$	71/23/6	74/22/4	31/67/2
	NH_4HCO_3	71/23/6	76/21/3	50/42/8
	$(NH_4)_2CO_3$	71/23/6	75/22/3	50/38/12
	$(NH_4)_2CO_3$[a]	75/25/0	77/23/0	79/21/0
ST-1	1,2-butanediol	71/23/6	81/15/4	65/19/16
	1-dodecanol	71/23/6	74/23/3	62/26/12
	1,4-butanediol	71/23/6	76/21/3	61/25/14
	1,4-butanediol[a]	75/25/0	78/22/0	87/13/0
ST-2	$Ce_{0.8}Mn_{0.15}Ba_{0.05}O_x$	80/15/5	84/12/4	72/17/11

[a] Supports calcined at 400 °C

and ST-2 catalysts are similar to each other. These arguments imply that the solvothermal method (ST-1 and ST-2) would be effective for preparing catalysts with highly dispersed Ba species on the surface. In the previous works [32, 37], we found that the activities of both the CeO_x–MnO_y–BaO and CeO_x–FeO_y–BaO catalysts closely correlate with the CO_2 uptakes of the catalysts. Therefore, these highly dispersed Ba species act as the adsorption sites for NO and contribute to the deNO_x activities.

Figure 5 shows the Mn 2p XPS spectra of the CP, ST-1, and ST-2 catalysts whose activities are shown in Fig. 4. All the samples exhibited Mn $2p_{3/2}$ and Mn $2p_{1/2}$ peaks at ~641 and ~652 eV, respectively. The shoulder peak at ~ 656 eV was attributed to the Ba(MNN) Auger peak [38]. The XPS spectra of the reference samples of Mn_3O_4 and MnO_2 exhibited the Mn $2p_{3/2}$ peak at ~641.2 and ~642.3 eV, respectively. The Mn $2p_{3/2}$ BEs of MnO, Mn_2O_3, and MnO_2 were reported to be 640.9, 641.8, and 642.5 eV, respectively [39]. These results indicate that the average valence of the Mn species in the present catalysts was lower than that in Mn_3O_4, the catalysts having an electron-rich Mn structure. These results are in accordance with the finding reported by Imamura et al. [40], who found that the addition of a small amount of cerium ions to manganese oxide remarkably affected its oxidation state. It must be noted that the catalyst having higher activity exhibited Mn 2p XPS peak at lower BE.

Raman spectra of the supports (Fig. 6A), supports calcined at 800°C without Ba (Fig. 6B), and catalysts (Fig. 6C) prepared by the three methods as well as Mn references (Fig. 6D) are shown in Fig. 6. For the cerium-containing samples, a Raman peak was observed at ~457 cm^{-1} due to the F_{2g} active mode of CeO_2 [41, 42]. A slight shift from the peak position for pure CeO_2 (462.2 cm^{-1}) is due to the incorporation of Mn ions in the CeO_2 matrix. Note, however, the peak position was not affected by the concentration of Mn ions in the CeO_2 matrix [36, 42]. In addition, all the supports and catalysts

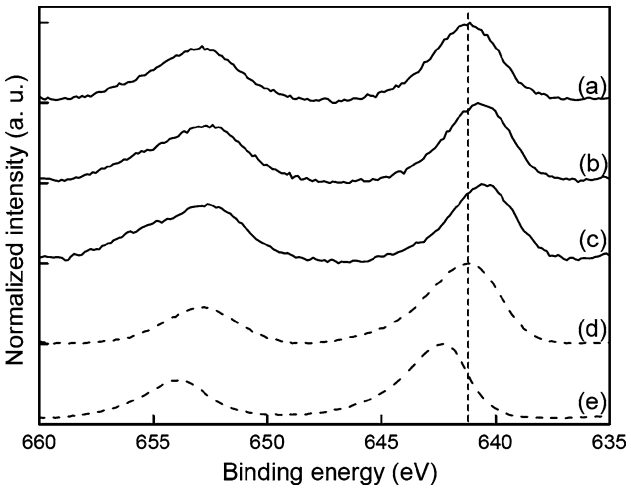

Fig. 5 Mn2p XPS spectra of: (*a*), CP($(NH_4)_2CO_3$); (*b*), ST-1(1,4-butanediol); (*c*), ST-2($Ce_{0.8}Mn_{0.15}Ba_{0.05}O_x$); (*d*), Mn_3O_4; (*e*), MnO_2

exhibited a peak at ~256 cm^{-1}, which is attributed to the defect space including an oxygen vacancy in the fluorite structure [43]. The supports also had peaks at ~315, ~638, and/or ~648 cm^{-1}, which were attributed to the Mn_2O_3 (~313 and ~639 cm^{-1}; Fig. 6D) and Mn_5O_8 (~648 cm^{-1} [44]) phases. The CP and ST-1 supports calcined at 800 °C (without Ba) exhibited a Raman peak at ~653 cm^{-1} (Fig. 6B) due to the Mn_3O_4 phase (Mn_3O_4 exhibits a peak at ~655 cm^{-1} as shown in Fig. 6D), indicating that the Mn_3O_4 phase was formed by thermal reduction of the Mn_2O_3 phase. These Mn phases were not detected by the XRD patterns, suggesting that they are highly dispersed on the support surface.

For the catalysts (Fig. 6C), Raman peaks were also observed at ~409, ~633, and ~653 cm^{-1}, which may be due to the $BaMnO_{3-\delta}$ phase [45] detected by the XRD study. This phase seems to have been formed by the reaction of highly dispersed Mn species with $Ba(NO_3)_2$. However, the surface Ba/Mn ratios of the catalysts were much lower than that expected from the chemical formula

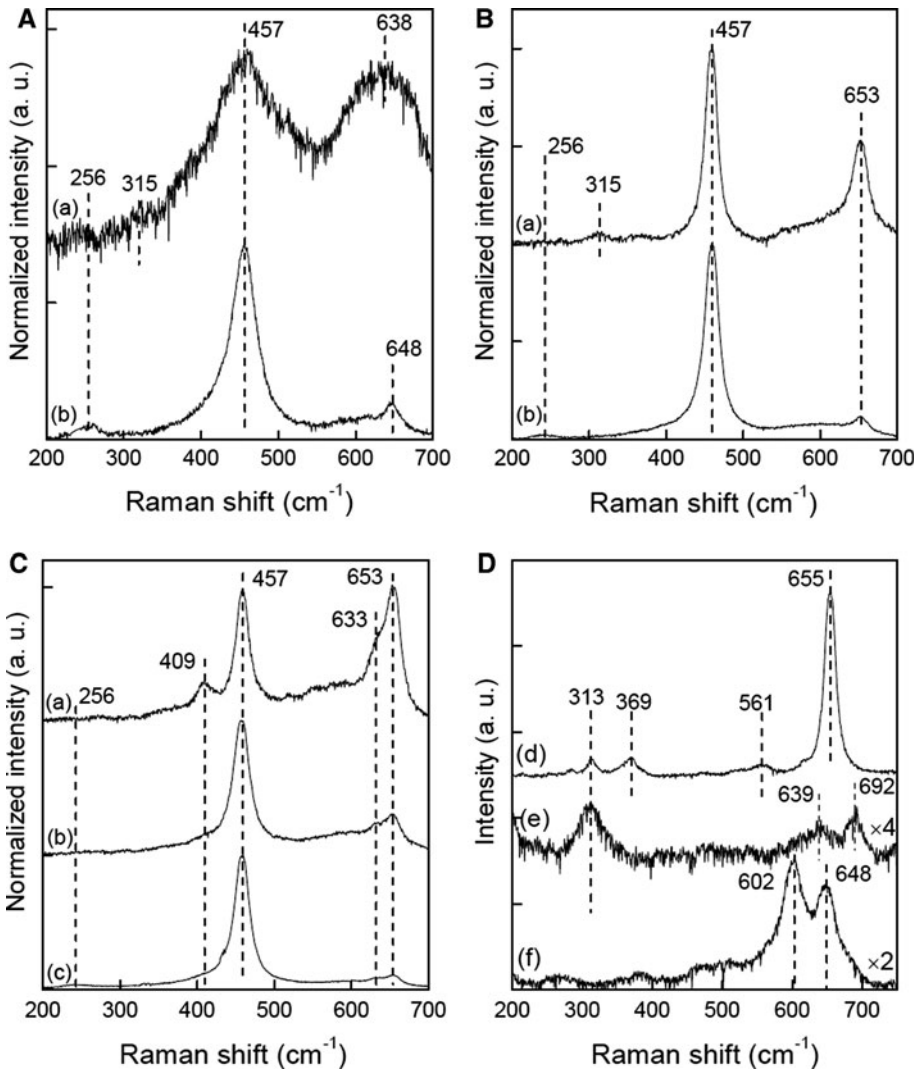

Fig. 6 Raman spectra of the supports (**A**), supports calcined at 800 °C without Ba (**B**), and catalysts (**C**); together with Mn reference samples (**D**): (*a*), CP($(NH_4)_2CO_3$); (*b*), ST-1(1,4-butanediol); (*c*), ST-2($Ce_{0.8}Mn_{0.15}Ba_{0.05}O_x$); (*d*), Mn_3O_4; (*e*), Mn_2O_3; (*f*), MnO_2

of $BaMnO_{3-\delta}$. Therefore, the Mn_3O_4 phase seems to be present on the surface of the catalyst, and the peak at ~653 cm^{-1} may overlap with the peak due to the Mn_3O_4 species, although the intensity of this peak increased by the addition of $Ba(NO_3)_2$.

The intensity ratio of the peak at ~653 to that at ~457 cm^{-1} (denoted as I_{653}/I_{457}) indicates the relative proportion of Mn-containing species ($BaMnO_{3-\delta}$ and/or Mn_3O_4) in the catalyst. Table 4 shows the effect of the preparation methods on the I_{653}/I_{457} ratio. The CP catalyst had a high I_{653}/I_{457} value, indicating that large amounts of the $BaMnO_{3-\delta}$ and/or Mn_3O_4 phases were present in this catalyst. This feature is in good agreement with the high Mn content on the surface of this catalyst (Table 3). The I_{653}/I_{457} values of the ST-1 and ST-2 catalysts are smaller than that of the CP catalyst, indicating that the solvothermal reaction was suitable for the synthesis of Ce–Mn mixed oxides because lesser amounts of $BaMnO_{3-\delta}$ and/or Mn_3O_4 phases are formed. It must be noted that the ST-2 catalyst contained a smaller amount of these phases than the ST-1 catalyst, indicating that the $BaMnO_{3-\delta}$ phase is not a catalytically active phase.

Table 4 Raman results for the ST-1, ST-2, and CP catalysts

Sample		I_{653}/I_{457} (%)[a]	I_{256}/I_{457} (%)[b]
CP	$(NH_4)_2CO_3$	112	2.0
	$(NH_4)_2CO_3$[c]	–	4.1
ST-1	1,4-butandiol	30	2.2
	1,4-butandiol[c]	–	8.3
ST-2	$Ce_{0.8}Mn_{0.15}Ba_{0.05}O_x$	10	2.7

[a] I_{653} : peak intensity at 653 cm^{-1}, I_{457} : peak intensity at 457 cm^{-1} (Raman spectrum)

[b] I_{256} : peak intensity at 256 cm^{-1}, I_{457} : peak intensity at 457 cm^{-1} (Raman spectrum)

[c] Supports calcined at 400 °C

In a previous work [36], we found that incorporation of Mn^{2+} in the fluorite structure of CeO_2 causes an increase in

the concentration of oxygen vacancies. As mentioned above, the oxygen vacancy was detected by a broad peak at ~256 cm^{-1}. The intensity ratio of the peak at ~256 to that at ~457 cm^{-1} (denoted as I_{256}/I_{457}) indicates the relative concentration of oxygen vacancies in the catalysts (Table 4). The correlation between the I_{256}/I_{457} value and the BE of Mn $2p_{3/2}$ peak of the catalyst is shown in Fig. 7, where the correlation between NO conversion and the BE of Mn $2p_{3/2}$ peak of the catalyst is also shown. The BE of the Mn 2p peak of the ST-2($Ce_{0.8}Mn_{0.15}Ba_{0.05}O_x$) catalyst was much lower than those for the ST-1 and CP catalysts, and the highest NO conversion was attained by the ST-2 catalyst having the lowest Mn 2p BE. In addition, a good correlation was also observed between the I_{256}/I_{457} value and the BE of Mn $2p_{3/2}$ peak of the catalyst, indicating that electron-rich Mn species incorporated in the fluorite structure have an important role in the formation of oxygen vacancies. In a previous paper [46], we examined the correlation between NO decomposition activities and physical properties of the CeO_x–FeO_y–BaO catalyst and found that data for both the CeO_x–MnO_y–BaO and CeO_x–FeO_y–BaO catalysts form one correlation line in the activity–vs.–oxygen vacancy concentration plot. Form these results, we concluded that neither Mn nor Fe component directly participates to the NO decomposition activities but both the components contribute to the formation of oxygen vacancies in the CeO_2 lattice, which play a key role in deriving NO decomposition activities of the catalysts [36]. The present results also suggest that incorporation of Mn ions in the ceria structure strongly depends on the preparation method of the mixed oxide.

A schematic comparison of the structures of the catalysts prepared by different methods is depicted in Fig. 8. The catalysts prepared by the co-precipitation method expose a large amount of the Mn-containing species on the surface of the catalyst. On the other hand, the catalyst

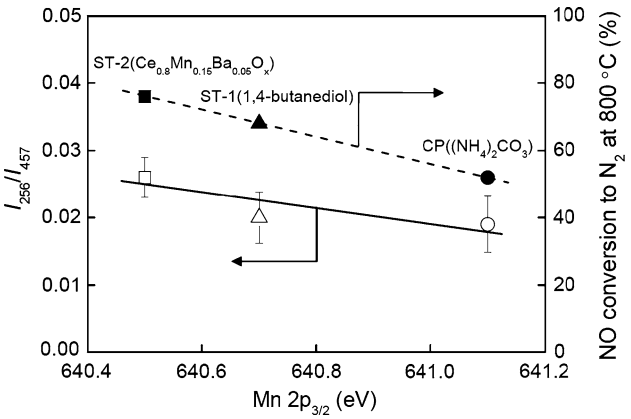

Fig. 7 Dependence of I_{256}/I_{457} value (*open symbols*) and NO conversion activity (*closed symbols*) of the CP (*circle*), ST-1 (*triangle*), and ST-2 (*square*) catalysts on the Mn $2p_{3/2}$ binding energy

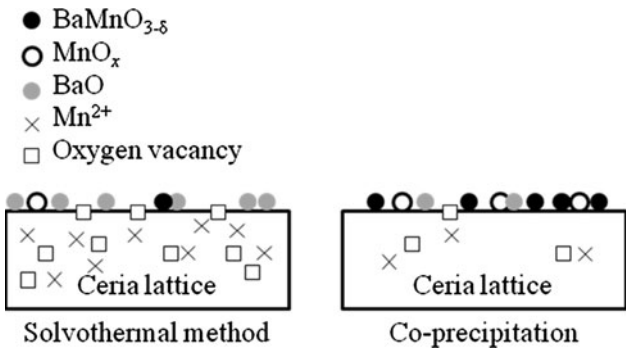

Fig. 8 Schematic comparison of the structures of the catalysts prepared by solvothermal and co-precipitation methods

prepared by the solvothermal method has only a low concentration of Mn on the surface, which inhibits the formation of the $BaMnO_{3-\delta}$ phase, thus maintaining highly dispersed Ba species. The solvothermal method, therefore, is effective for preparing highly efficient catalysts for direct decomposition of NO.

4 Conclusions

The CeO_x–MnO_y–BaO catalysts were prepared by solvothermal (ST-1, ST-2) and co-precipitation (CP) methods and their direct NO decomposition activities were investigated. The Raman and XPS results indicate that the CP catalysts had larger amounts of $BaMnO_{3-\delta}$ and/or Mn_3O_4 phases on the catalyst surface, while the characterization suggests the presence of highly dispersed Ba species on the ST-2 catalyst. Among the catalysts examined, the highest NO conversion to N_2 was attained by the ST-2($Ce_{0.8}Mn_{0.15}Ba_{0.05}O_x$) catalyst. This catalyst exhibits a Mn 2p XPS peak at the lowest binding energy. This fact suggests that a large amount of Mn^{2+} is incorporated in the CeO_2 matrix leading to the formation of oxygen vacancies. The solvothermal reaction is suitable for synthesizing Ce–Mn mixed oxides.

Acknowledgments We are grateful to Prof. Takeshi Abe of Kyoto University for his help in Raman spectra measurements and Dr. Seiichiro Imamura and Dr. Hiroyoshi Kanai of Kyoto University for their invaluable advice.

References

1. Trovarelli A (1996) Catal Rev Sci Eng 38:439
2. Chen H, Sayari A, Adnot A, Larachi F (2001) Appl Catal B 32:195
3. Qi GS, Yang RT, Chang R (2004) Appl Catal B 51:93
4. Machida M, Uto M, Kurogi D, Kijima T (2000) Chem Mater 12:3158
5. Rao T, Shen MQ, Jia LW, Hao JJ, Wang J (2007) Catal Commun 8:1743

6. Tang XF, Li YG, Huang XM, Xu YD, Zhu HQ, Wang JG, Shen WJ (2006) Appl Catal B 62:265
7. Yu DQ, Liu Y, Wu ZBA (2010) Catal Commun 11:788
8. Wu YS, Zhang YX, Liu M, Ma ZCC (2010) Catal Today 153:170
9. Delimaris D, Ioannides T (2008) Appl Catal B 84:303
10. Qi GS, Yang RT (2004) J Phys Chem B 108:15738
11. Kaneko H, Miura T, Ishihara H, Taku S, Yokoyama T, Nakajima H, Tamaura Y (2007) Energy 32:656
12. Amirnazmi A, Benson JE, Boudart M (1973) J Catal 30:55
13. Wu RJ, Chou TY, Yeh CT (1995) Appl Catal B 6:105
14. Miller DD, Chuang SSC (2009) J Phys Chem C 113:14963
15. Winter ERS (1971) J Catal 22:158
16. Huang SJ, Walters AB, Vannice MA (2000) J Catal 192:29
17. Iwamoto M, Yahiro H, Mine Y, Kagawa S (1989) Chem Lett 18:213
18. Iwamoto M, Hamada H (1991) Catal Today 10:57
19. Groothaert MH, Bokhoven JA, Battiston AA, Weckhuysen BM, Schoonheydt RA (2003) J Am Chem Soc 125:7629
20. Park PW, Kil JK, Kung HH, Kung MC (1998) Catal Today 42:51
21. Haneda M, Kintaichi Y, Bion N, Hamada H (2003) Appl Catal B 46:473
22. Teraoka Y, Fukuda H, Kagawa S (1990) Chem Lett 19:1
23. Teraoka Y, Harada T, Kagawa S (1998) J Chem Soc Faraday Trans 94:1887
24. Ishihara T, Ando M, Sada K, Takiishi K, Yamada K, Nishiguchi H, Takita Y (2003) J Catal 220:104
25. Iwakuni H, Shinmyou Y, Yano H, Matsumoto H, Ishihara T (2007) Appl Catal B 74:299
26. Zhu JJ, Xiao DH, Li J, Yang XG (2009) Catal Lett 129:240
27. Imanaka N, Masui T, Masaki H (2007) Adv Mater 19:3660
28. Tsujimoto S, Mima K, Masui T, Imanaka N (2010) Chem Lett 39:456
29. Goto K, Matsumoto H, Ishihara T (2009) Top Catal 52:1776
30. Iwamoto S, Yasuda T, Inoue M (2002) Adv Technol Mater Mater Proc J 4:58
31. Iwamoto S, Takahashi R, Inoue M (2007) Appl Catal B 70:146
32. Hong W-J, Iwamoto S, Inoue M (2011) Catal Today 164:489
33. Inoue M, Nishikawa T, Otsu H, Kominami H, Inui T (1998) J Am Ceram Soc 81:1173
34. Inoue M, Nishikawa T, Kominami H, Inui T (2000) J Mater Sci 35:1541
35. Hosokawa S, Iwamoto S, Inoue M (2008) Mater Res Bull 43:3140
36. Hong W-J, Iwamoto S, Hosokawa S, Wada K, Kanai H, Inoue M (2011) J Catal 277:208
37. Hong W-J, Iwamoto S, Inoue M (2010) Catal Lett 135:190
38. Muilenberg GE (1979) Handbook of X-ray photoelectron spectroscopy. Perkin-Elmer Corporation, Minnesota, p 139
39. Lopez-Navarrete E, Caballero A, Gonzalez-Elipe AR, Ocana M (2004) J Eur Ceram Soc 24:3057
40. Imamura S, Shono M, Okamoto N, Hamada A, Ishida S (1996) Appl Catal A 142:279
41. Reddy BM, Khan A (2005) Catal Surv Asia 9:155
42. Arena F, Trunfio G, Negro J, Fazio B, Spadaro L (2007) Chem Mater 19:2269
43. Nakajima A, Yoshihara A, Ishigame M (1994) Phys Rev B 50:13297
44. Gao T, Norby P, Krumeich F, Okamoto H, Nesper R, Fjellvag H (2010) J Phys Chem C 114:922
45. Roy C, Budhani RC (1998) Phys Rev B 58:8174
46. Hong W-J, Iwamoto S, Hosokawa S, Wada K, Kanai H, Inoue M (2011) Appl Catal B 106:142